Jet noise prediction using a sweeping based turbulence generation process

A. Lafitte[a], E. Laurendeau[b], T. Le Garrec[c] and C. Bailly[d]

[a]Liebherr Aerospace, 29 avenue de la division Leclerc, 92320 Chatillon, France
[b]Liebherr Aerospace, 408 avenue des Etats-Unis, 31016 Toulouse, France
[c]Onera, Département de Simulation Numérique des Ecoulements et Aéroacoustique, BP 72 - 29, avenue de la Division Leclerc, 92322 Chatillon Cedex
[d]Laboratoire de Mecanique des Fluides et d'Acoustique, 36 Av Guy de Collongue 69134 Ecully Cedex
anthony.lafitte@onera.fr

A predictive tool for acoustics of confined subsonic jets, developped in the framework of a PhD thesis funded by Liebherr Aerospace (LTS) and hold at Onera, is presented in this paper. An hybrid method, combining turbulence generation by a stochastic model, and acoustic propagation by an Euler solver is there used. A new combined approach based on the sweeping hypothesis to generate isotropic turbulent fields starting from a steady RANS computation is introduced. In addition of allowing the modeling of space-time velocity correlation functions and the preservation of the turbulent kinetic energy spatial distribution, it integrates mean flow effects on the turbulent velocity field (AIAA paper 2011-2888). This stochastic model has been coupled with Onera's Euler solver *sAbrinA_v0* and the resulting tool has been tested on a subsonic free jet with a nozzle diameter $D = 80$mm at Mach number 0.72. Numerical spectra in the far-field are compared to experimental data available at Onera.

1 Introduction

Liebherr Aerospace (LTS) develops air management systems for the aeronautic industry. Those devices ensure the bleed, cooling, drying and transportation of conditioned air to the cabins of aircrafts. In order to optimize its products, LTS works on different modifications on those packs to make them more energy efficient. One of these concepts is to integrate jet pumps which could offer significant gains over the current technologies for various functions of the systems. Assuming that these devices could contribute directly to ramp noise, the use of a numerical tool to predict acoustics of jet pumps could help to propose, if the need arises, appropriate noise reduction solutions.

The work presented in this paper is a part of an extended study to build such a tool. Considering that methodologies based on unsteady computations are still too complex to be extensively used in industrial contexts, the chosen methodology is based on stochastic methods which present the advantage to be easily usable and less expensive in CPU hours. The idea is to synthetise a turbulent velocity field from a steady RANS computation to calculate acoustic source terms to inject in acoustic propagation equations.

A new stochastic approach which takes the sweeping effect into account, or the fact that small scale turbulent structures are advected by larger eddies, is presented in the section I as well as results of its validation. The coupling of this stochastic method with Onera's Euler solver is introduced in the section II. Acoustic results obtained by studying a subsonic jet at Mach 0.72 with the developed tool are shown in the section III.

2 Turbulence generation process

The stochastic methods allow, for a configuration of interest, to generate synthetic turbulence knowing the mean flow and transport variables provided by a preliminary steady RANS computation. Since the former model proposed by Kraichnan[1], stochastic methods have been widely developed and used in fields as diverse as particle diffusion[1, 2], turbulence initialization for LES application[3, 4] or aeroacoustics[5, 6, 7, 8]. The model presented in this section proposes to take the sweeping hypothesis into account[9].

2.1 Sweeping based stochastic model

The sweeping effect, stating that inertial range structures are advected by the energy containing eddies, is suspected to play a predominant role in the acoustic emission of a subsonic jet. The modeling of this phenomenom implies a separation in the turbulence scales. Following the former idea of Fung *et al.*[2], the turbulent velocity field $\mathbf{u}$ is splitted into two parts : a term $\mathbf{u}_l$ linked to the large scale eddies and a term $\mathbf{u}_s$ associated to small scale structures:

$$\mathbf{u}(\mathbf{x}, t) = \mathbf{u}_l(\mathbf{x}, t) + \mathbf{u}_s(\mathbf{x}, t) \tag{1}$$

Starting from the homogenous isotropic turbulence hypothesis, a Von Kármán-Pao spectrum is imposed at each point of the grid depending on the local turbulent kinetic energy. This energy spectrum is discretised linearly by N modes of wave number k_n distributed between k_{min} and k_{max} so that the step size Δk is constant. As shown in the Figure 1, the separation in the turbulence scales is achieved by introducing a space dependent cut-off wave number $\mathbf{k}_c$. The modes with $k_n \leq k_c$ contribute to $\mathbf{u}_l$ and those with $k_n > k_c$ to $\mathbf{u}_s$.

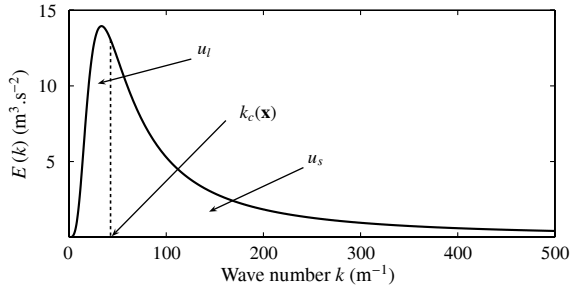

Figure 1: Von Kármán-Pao spectrum showing the respective contribution of $\mathbf{u}_l$ and $\mathbf{u}_s$.

In one hand, the term associated to the large scale structures defined in equation (2) is as a sum of N_l Fourier modes [5] defined by an amplitude $A_n = \sqrt{E(k_n)\Delta k}$, a random phase φ_n and a direction σ_n. Information relative to the set up of these variables can be found in the literature[5, 9, 10]. $\mathbf{u}_l$ being defined locally, the convection velocity $\mathbf{u}_c$ allows to model the displacement of the turbulent modes downstream of the flow.

$$\mathbf{u}_l(\mathbf{x}, t) = 2 \sum_{n=1}^{N_l} A_n \cos\left(\mathbf{k}_n (\mathbf{x} - \mathbf{u}_c t) + \omega_n t + \varphi_n\right) \boldsymbol{\sigma}_n \tag{2}$$

$\mathbf{u}_c$ needs imperatively to be a constant on space in order to avoid a decorrelation of the generated velocity field at large times[13]. Accordingly to the literature[11], $\mathbf{u}_c$ is set to $0.6U_j$ for jet applications, where U_j is the jet velocity at the nozzle exit. The Kolmogorov pulsation is chosen for ω_n since it is the most appropriate choice for low wave numbers[12]. As for $\mathbf{u}_l$, ω_n is a constant of space and is computed using a mean value of the dissipation rate: $\omega_n = C_k^{1/2} < \varepsilon >^{1/3} k_n^{2/3}$ where $< . >$ designates the average over the whole source domain.

On the other hand, $\mathbf{u}_s$ is modeled using a modified Billson approach[6] and is written as a sum of two terms:

$$\mathbf{u}_s(\mathbf{x},t) = a(\mathbf{x})\,\mathbf{v}(\mathbf{x},t) + b(\mathbf{x})\,\boldsymbol{\zeta}(\mathbf{x},t) \tag{3}$$

The modeling of the sweeping effect is introduced in equation (3) through the computation of the field $\mathbf{v}$. At a given iteration, $\mathbf{v}$ is the velocity field $\mathbf{u}_s$ at the previous iteration $\mathbf{u}_s^{it-1}$ convected by the vector field $\left(\overline{\mathbf{u}} + \mathbf{u}_l^{it-1}\right)$.In other terms, $\mathbf{v}$ is solution of the advection equation (4):

$$\frac{\partial \mathbf{u}_s^{it-1}}{\partial t} + \left(\overline{\mathbf{u}} + \mathbf{u}_l^{it-1}\right)\cdot\nabla\mathbf{u}_s^{it-1} = \mathbf{0} \tag{4}$$

In equation (3), $\boldsymbol{\zeta}$ is a sum of $N_s = N - N_l$ spatial Fourier modes regenerated at each iteration so that it is a locally white noise:

$$\boldsymbol{\zeta}(\mathbf{x}) = 2\sum_{n=N_l+1}^{N} A_n \cos\left(\mathbf{k}_n\cdot\mathbf{x} + \varphi_n\right)\boldsymbol{\sigma}_n \tag{5}$$

The choice of $a = e^{-\Delta t/\tau}$ imposes the temporal decorrelation, while $b = \sqrt{1-a^2}$ allows a conservation of the turbulent kinetic energy in homogenous media.

2.2 Model validation

The objective of the extended project is to study a confined jet. According to the fact that such a configuration is too complex to be investigated at first and that it has not been widely studied aerodynamically and acoustically, the validation work focuses on the aerodynamic of a free jet[9]. Particularly, the velocity correlation functions defined by equation (6) are checked in the shear layer at various axial locations.

$$R_{ij}(\boldsymbol{x},\boldsymbol{r},\tau) = \frac{\overline{u_i(\boldsymbol{x},t)u_j(\boldsymbol{x}+\boldsymbol{r},t+\tau)}}{\sqrt{\overline{u_i(\boldsymbol{x},t)^2}}\sqrt{\overline{u_j(\boldsymbol{x}+\boldsymbol{r},t+\tau)^2}}} \tag{6}$$

A RANS computation performed at Onera of the Φ_{80} jet, which is a cold subsonic jet at Mach 0.72 with a nozzle diameter D = 80mm, has been used to feed the stochastic model. 2D restricted regular cartesian grids have been extracted at different locations of the shear layer and on the jet axis.

Table 1: Simulation parameters.

	Point P_1	**Point P_2**
Position (x, y)	$(2D; 0.5D)$	$(6.5D; 0.5D)$
Grid dimensions	161×61	181×81
Grid size Δ	1 mm	2 mm
Number of modes	80	80
k_{max}	1000 m^{-1}	500 m^{-1}
Δt	2.10^{-6}s	4.10^{-6}s

Results obtained at two different points located in the center of the shear layer are shown in this paper and compared to experimental data obtained by Fleury *et al.*[11]. Simulation parameters are sumarized in Tab 1. Equation (4) is solved using a low-storage 2^{nd} order optimized Runge-Kutta of Bogey & Bailly[14] with six understages and a 11 points 4^{th} order optimized DRP scheme. A 11 points 4^th order spatial filtering is applied as well. Tam and Dong's radiation boundary condition is set at the inlet of the computation domain while outflow boundary conditions are imposed at the outlets. For both grids, a simulation consists of 30 000 temporal iterations and numerical results have been obtained by averaging 10 simulations in order to increase the statistics.

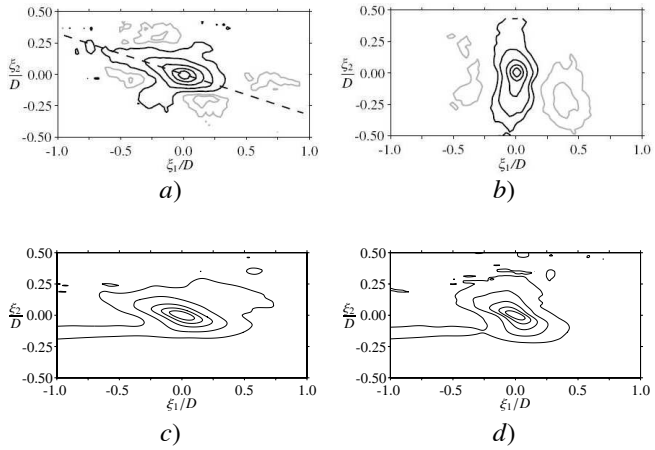

Figure 2: On the top: experiments[11]. On the bottom : Numerical results. *a)* and *c)* refers to the isocontours of $R_{11}(x,r,0)$. *b)* and *d)* refers to the isocontours of $R_{22}(x,r,0)$. The distance $r = \sqrt{\xi_1^2+\xi_2^2}$. R_{11} levels:(0.05,0.2,0.4,0.6,0.8), R_{22} levels: (0.1,0.2,0.4,0.6,0.8).

The sweeping based stochastic model is able to reproduce the space correlation functions $R_{ij}(x,r,0)$ as it is shown in Figure 2. The inclination of the R_{11} pattern is correctly modeled, proof that the approach takes correctly into account the mean flow effects on the turbulent velocity field. The mean convection velocity of the turbulent structures in the shear layer which corresponds to the slope of the plot in Figure 3 representing the displacement of the correlation pattern center with the increasing of the time delay τ is correctly modeled as well.

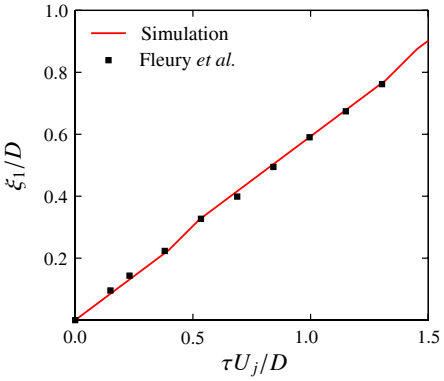

Figure 3: Dispacement of the maximum of $R_{11}(x,t,\tau)$ versus the adimensionalized time delay τ at the point P_2

The decorrelation of the velocity field is shown at the point P_2 in different frames in the Figure 4. The method offers a better modeling of this process in the Lagrangian frame than in the Eulerian frame.

A comparison of the reconstructed turbulent kinetic energy - computed by $1/2(\overline{u_1^2}+\overline{u_2^2}+\overline{u_3^2})$ - with the energy injected from the Von Kármán-Pao spectra $\overline{k} = \int_{k_{min}}^{k_{max}} E(k)\delta k$ is plotted in Figure 5. Results show a slight loss of energy for each profile. This loss occurs during the resolution of the equation (4) because of the inhomogeneity in $\overline{k}$ of the medium. Equation (4) implies that, at a given point, $\mathbf{u}_s$ depends on turbulence built from upstream conditions plus a certain amount of local

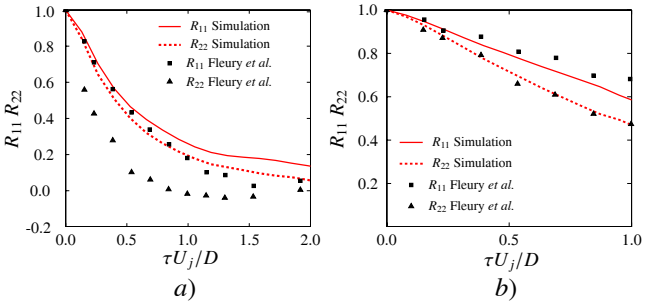

Figure 4: Decorrelation of the stochastic velocity field: *a*) in an Eulerian frame, *b*) in a Lagrangian frame moving at the velocity $u_c = 0.6U_j$

energy. So if the TKE is not a constant of space, the injected energy can not be exactly recovered from the stochastic velocity field. Nevertheless, the locations of the respective maximum as well as the global shape of the profiles are reproduced. The spatial distribution of the most energetic points is therefore preserved.

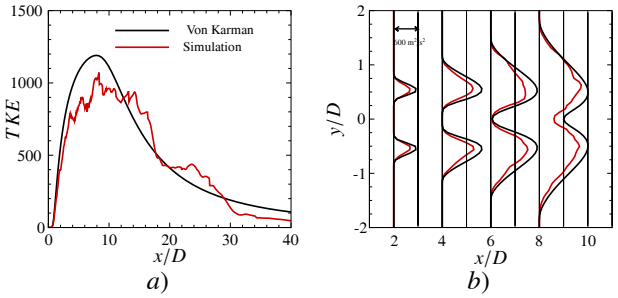

Figure 5: Comparison between the reconstructed and the initial turbulent kinetic energy. *a*) Profile along the $y = 0.5D$ axis, *b*) radial profiles for various longitudinal position x.

In contrary to methods exclusively formulated in Fourier modes, this approach is able to model the space-time velocity correlation functions which are closely linked to the "size" and temporal evolution of the acoustic sources[9]. It allows to limit the loss of turbulent kinetic energy that occured using a Billson approach as well. In addition, it allows to deal with 3-D complex geometries.

3 Acoustic propagation modeling

The stochastic model presented in section 2 is coupled with Onera's Euler solver *sAbrinA_v0* in order to calculate the acoustic propagation. The idea is to force non linear terms in the LEE using the synthetised velocity field and to use the Euler equations as a linear propagator.

3.1 Description of Euler solver *sAbrinA_v0*

The CAA calculations were conducted with ONERA's *sAbrinA_v0* solver [15, 16]. *sAbrinA_v0* is a structured grid, time-accurate CAA code that solves either the full or the linear Euler equations, in a conservative and perturbed form (with a splitting of the complete variables into a "frozen" mean flow and a "fluctuating" perturbation). The solver employs high-order, finite-difference operators, involving 6th-order spatial derivatives and 10th-order filters, as well as a 3rd-order, multi-stage, Runge-Kutta time-marching scheme. The code deals with multi-block structured grids with one-to-one interfaces, and is fully parallelized using the Message Passing Interface (MPI) standard. Finally, the solver includes the usual boundary conditions (reflection by solid walls, non-reflecting / free-field radiation [15, 16, 17], etc.), as well some unique to specific applications (such as the surface coupling technique [15, 16]). Finally, it can be pointed out that such CAA solver is parallelized (in a MPI - Message Passing Interface sense), which offered to run the present calculations in parallel. More detailed information about the *sAbrinA_v0* solver and its underlying methodology can be found in Ref.[15, 16].

One can remind that the free-field radiation through peripheral boundaries is mimicked with the help of an as simple as efficient technique; originally proposed in Ref. [15, 16] and accurately assessed / validated in Ref.[17], such technique is based on a progressive decreasing of the spatial derivatives / filters accuracy order (to be obtained via a reduction of the schemes stencil half-width). Coupled with a rapid grid stretching (over 6 peripheral rows of ghost points), this trick allows the perturbations to leave properly the calculation domain - that is to say without generating significant numerical reflections at the frontiers.

3.2 Formulation of the Euler equations

In the present work, a source term S_i is used to force the perturbative linearized Euler equations in conservative form:

$$\frac{\partial \rho'}{\partial t} + \frac{\partial}{\partial x_j}\left(\rho u_j' + \rho' \overline{u}_j\right) = 0 \tag{7}$$

$$\frac{\partial (\rho u_i)'}{\partial t} + \frac{\partial}{\partial x_j}\left(\rho' \overline{u}_i \overline{u}_j + \overline{\rho}\,\overline{u}_i u_j' + \overline{\rho}\,\overline{u}_j u_i' + p' \delta_{ij}\right) = S_i \tag{8}$$

$$\begin{aligned}\frac{\partial (\rho e_0)'}{\partial t} + \frac{\partial}{\partial x_j}\Bigg[u_j'\left(\frac{1}{2}\overline{\rho}\,\overline{u}_k\overline{u}_k + \frac{\gamma}{\gamma-1}\overline{p}\right) \\ + \overline{u}_j\left(\overline{\rho}\,\overline{u}_k u_k' + \frac{1}{2}\rho'\overline{u}_k\overline{u}_k + \frac{\gamma}{\gamma-1}p'\right)\Bigg] = 0\end{aligned} \tag{9}$$

The capability of this set of equations to preserve the multipolar feature of a source and to take the mean flow effects into account has been checked by computing the 2D test cases proposed by Bailly and Juvé[18] on a 400×400 cartesian grid. First, a dipolar distribution F_i has been injected in the LEE: $F_i = S_i$.

$$\begin{cases} F_1 = \varepsilon \cos\left(\frac{\pi}{10}x\right) e^{-\alpha y^2} \sin(\omega t) \\ F_2 = 0 \\ (x, y) \in [-5; 5] \times \Re \end{cases} \tag{10}$$

In equation (10), the amplitude ε is equal to 0.01, $\omega \Delta t = 2\pi/60$ and the coefficient $\alpha = \log(2)/5$. Results obtained with *sAbrinA_v0* are compared to the analytical solution given by $\rho' = -F_1 * G$ with G, the following Green function:

$$G(\mathbf{r}, t) = \frac{\partial}{\partial x}\left[\frac{i}{4c_0^2} H_0^1\left(\frac{\omega}{c_0} r\right) e^{-i\omega t}\right] \tag{11}$$

The pressure along the axis $y = 0$ is plotted for two different temporal iterations in Figure 6. Numerical results perfectly match the analytical solution. A quadrupolar distribution T_{ij} defined in equation (12) has been tested as well by imposing $S_i = \partial T_{ij}/\partial x_j$ and resolving the LEE around a

Bickley's bidimensionnal mean flow jet profile described by equation (13) :

$$T_{ij} = \varepsilon \frac{20}{\pi} \begin{bmatrix} -\cos\left(\frac{\pi}{20}x\right) e^{-\alpha y^2} & 0 \\ 0 & \cos\left(\frac{\pi}{20}y\right) e^{-\alpha x^2} \end{bmatrix} \sin(\omega t) \quad (12)$$

$$\frac{\overline{u}_1}{c_o} = \frac{0.5}{\cosh^2\left[(1+\sqrt{2})y/20\right]} \quad (13)$$

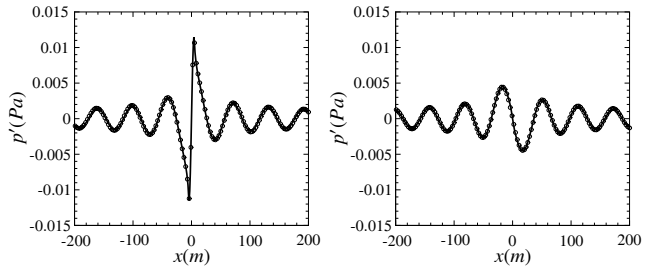

Figure 6: Dipolar distribution. Pressure profile along the axis $y = 0.5D$. ▬ Simulation, ∘ Analytical solution. *a*) $t = 560\Delta t$. *b*) $t = 720\Delta t$

The Figure 7 presents a comparison between a pressure snapshot taken from the present work and one obtained by Bailly and Juvé[18]. Both are in good agreement.

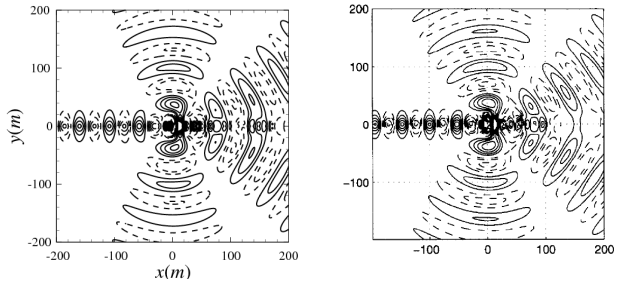

Figure 7: Quadrupolar distribution. Pressure fluctuations in the computational domain at $t = 640/(1+M)\Delta t$. *a*) Present work, *b*) Bailly and Juvé[18]. ▬ Positive values, from 0.001 to 0.011 Pa with a step size of 0.001, ▬ ▬ Negative values

These test cases show that the acoustic wave propagator is correctly reconstructed numerically from this set of linearized Euler equations. This wave propagator noticeably preserves the multipolar feature of a given source and integrates the mean flow effects.

3.3 Coupling stochastic model/sAbrinA_v0

In the present work, the term S_i is computed directly from the stochastic velocity field. The source term used in this paper is the one used in Ref. [19]:

$$S_i = -\frac{\partial \overline{\rho} u_i' u_j'}{\partial x_j} \quad (14)$$

At each iteration, the stochastic field **u** is first generated from equation (1). In a second time S_i is computed and then the forced linearized equations (7), (8) and (9) are resolved.

4 Acoustic prediction of a free jet

The numerical tool presented in sections 2 and 3 is applied to a free subsonic jet configuration. The RANS computation of the subsonic jet Φ_{80} presented in the section 2 has therefore been used to access the mean flow and transport variables needed to calculate the Von Kármán-Pao spectra and to resolve equations (4), (7), (8), and (9).

4.1 Computational setup

The computational grid consists of $361 \times 284 \times 184$ mesh points. The cartesian grid extends up to $30D$ in the flow direction and is bounded by $[-4D; 17D]$ in the $y-$direction and $[-4D; 4D]$ in the $z-$direction. Sizes of the smallest cell, located in the vicinity of the nozzle exit, are $\Delta x = 5$mm and $\Delta y = \Delta z = 2.5$mm. This spatial resolution, able to support an acoustic wave number $k_{max} = 200$ m^{-1}, is held up to 20 diameter in the $x-$direction. In the $y-$ and the $z-$direction, the finest resolution is held up to $2.5D$ from the jet axis. A damping zone has been set up from $x = 16D$ to the exit of the domain in order to avoid spurious reflections that could contaminate the final solution. A stretching of the mesh in the downstream direction is applied in this region in order to improve efficiency of the artificial numerical dissipation. The Von Kármaán-Pao spectra are discretised by 100 modes linearly distributed between $2 \leq k_n \leq k_{max} = 200$ m^{-1}. The time step Δt is set to 3.5×10^{-6}s based on a CFL number of 0.86. 30 000 temporal iterations are performed on 252 processors. Computation is achieved in approximately 30 hours.

4.2 Acoustic results

Pressure signals in the far-field are directly obtained from *sAbrinA_v0*. Associated power spectral densities are computed using 0.98 s of physical time with a sampling frequency of $1/10\Delta t$ and plotted in Figure 8 for 4 different observers located on an arc of radius $R = 10D$ from the nozzle exit.

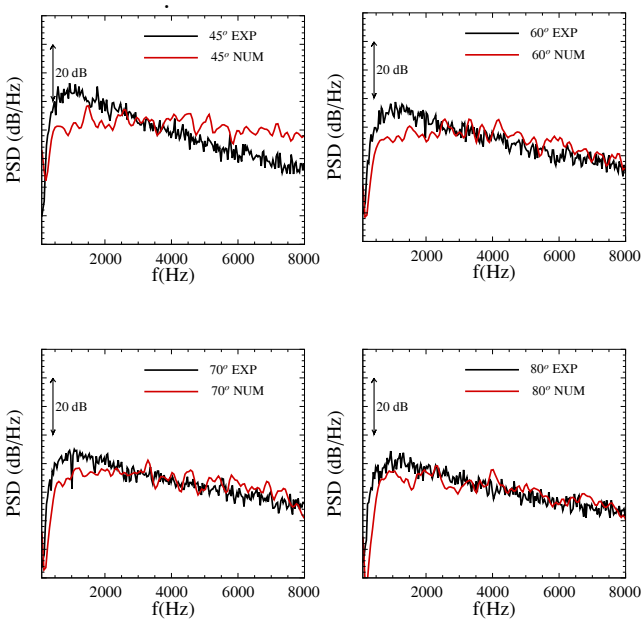

Figure 8: Power spectral density of the pressure signals for different observers located at $r = 10D$ from the nozzle exit.

Respective angles of the observers are $\theta = 45^o$, 60^o, 70^o, 80^o from the jet axis. Numerical spectra have been vertically shifted. The results are compared with Onera's experimental data for the Φ_{80} free jet.Regarding the Figure 8, one can notice that for the small angle (45^o), the global behaviour of the spectra is not correctly modeled. In particular, the slope at high frequencies is almost equal to zero and the spectrum does not show a clearly defined central frequency. The investigation of this issue is still in progress. Nevertheless, the more θ increases the more the numerical spectra fit the experimental curves. For large angles and noticeably for the observer located at $\theta = 80^o$, there is a good agreement between the simulation and the experiments. The slope at high frequencies and the central frequency are correctly modeled.

5 Conclusion

The present work presents a predictive tool for acoustics of subsonic jet flows. Starting from a steady computation, this approach allows to synthetise a turbulent velocity field to compute acoustic source term to inject in the linearized Euler equations.

The sweeping based stochastic method noticeably reproduces the velocity correlation functions in the flow and includes mean flow effects on the turbulence. The coupling of the sochastic model and Onera's Euler solver *sAbrinA_v0* is able to predict the acoustic radiation of a subsonic free jet at large angles. On-going study are still in progress to solve the problem for small angles prediction.

This approach presents the advantage of being easily usable and less expensive in CPU hours than direct computations. One can notice that it is applicable to any configuration as long as a steady computation of the flow is available to feed the stochastic method and that the considered turbulence physics is compatible with the hypotheses made to build the current numerical model.

The next step is to apply the method to the confined configuration. The present numerical tool will be used to model the near-fiel acoustic propagation, i.e inside the tube and in the vicinity of its exit. For CPU cost reduction, the far-field acoustics might be recovered using an integral method. The final tool will be validated by comparing numerical results with data obtained from an experimental campaign let by LTS at the Ecole Central Lyon in 2011 on a realistic jet pump with a single injector.

References

[1] R.H Kraichnan, "Diffusion by a random velocity field", *Phys. Fluids* **13**, 22-31 (1970)

[2] J.C.H. Fung, J.C.R. Hunt, N.A Malik, R.J. Perkins, "Kinematic simulation of homogeneous turbulence by unsteady random fourier modes", *J. Fluid Mech.* **236**, 281-318 (1992)

[3] S. Lee, S.K. Lele, P. Moin, "Simulation of spatially evolving turbulence and the applicability of Taylor's hypothesis in compressible flow", *Phys. Fluids A* **4**, 1521-1530 (1992)

[4] N. Jarrin, S. Benhamadouche, D. Laurence, R. Prosser, "A synthetic-eddy-method for generating in flow conditions for large-eddy simulation", *International Journal of Heat and Fluid Flow* **27**, 585-593 (2006)

[5] C. Bailly, D. Juvé, *5th AIAA/CEAS Aeroacoustics Conference*, AIAA Paper 99-1872, Seattle (1999)

[6] M. Billson, L.E. Eriksson, L. Davidson, *9th AIAA/CEAS Aeroacoustics Conference*, AIAA Paper 2003-3282, Hilton Head (2003)

[7] R. Ewert, "Broadband slat noise prediction based on CAA and stochastic sound sources from a fast Random Particle-Mesh (RPM) method", *Computers and Fluids* **37**, 369-387 (2008)

[8] M. Omais, B. Caruelle, S. Redonnet, E. Manoha, P. Sagaut, *14th AIAA/CEAS Aeroacoustics Conference*, AIAA paper 2008-2938, Vancouver (2008)

[9] A. Lafitte, E. Laurendeau, T. Le Garrec, C. Bailly, *17th AIAA/CEAS Aeroacoustics Conference*, AIAA Paper 2011-2888, Portland (2011)

[10] W. Béchara, C. Bailly, P. Lafon, S. Candel, "Stochastic approach to noise modeling for free turbulent flows", *AIAA Journal* **32**, 455-463 (1994)

[11] V. Fleury, C. Bailly, E. Jondeau, M. Michard, D. Juvé, "Space-time correlations in two subsonic jets using dual particle image velocimetry measurements", *AIAA Journal* **46**(10), 2498-2509 (2008)

[12] B. Favier, F.S. Godeferd, C. Cambon, "On space and time correlations of isotropic and rotating turbulence", *Phys. Fluids* **22**, 1-13 (2010)

[13] P. Batten, U. Goldberg, S. Chakravarthy, *8th AIAA/CEAS Aeroacoustics Conference*, AIAA Paper 2002-2511, Breckenridge (2002)

[14] C. Bogey, C. Bailly, "A family of low dispersive and low dissipative explicit schemes for flow and noise computations", *J. Comput. Phys.* **194**, 194-214 (2004)

[15] S. Redonnet, E. Manoha, P. Sagaut, *7th AIAA/CEAS Aeroacoustics Conference*, Maastricht (2001)

[16] S. Redonnet, *PhD Thesis*, Université de Bordeaux (2001)

[17] R. Guenanff, *PhD Thesis*, Université de Rennes (2004)

[18] C. Bailly, D. Juvé, "Numerical solution of acoustic propagation problems using linearized Euler equations", *AIAA Journal* **38**(1), 22-29 (2000)

[19] C. Bogey, C. Bailly, D. Juvé, "Computation of flow noise using source terms in linearized Euler's equations", *AIAA Journal* **40**(2), 235-243 (2002)